




Article

Properties of Unburned Brick Produced by Entirely Waste-Stream Binder Activated by Desulfurization Gypsum

Lei Zhang ^{1,2}, Lijie Guo ^{1,2,*} , Yue Zhao ^{1,2}  and Mengyuan Li ^{1,2} ¹ BGRIMM Technology Group, Beijing 100160, China² National Centre for International Research on Green Metal Mining, Beijing 102628, China

* Correspondence: guolijie@bgrimm.com

Abstract: The massive accumulation of industrial solid wastes such as circulating fluidized bed fly ash (CFA), silicon-calcium slag (SCS), and desulfurization gypsum (FGD) occupy land resources and bring varying degrees of pollution to soil, water, and atmosphere. Unburned brick is a new construction material prepared from industrial waste residues such as fly ash and tailings without high-temperature calcination. It has excellent potential in consuming large quantities of industrial solid waste. In this paper, 70% of CFA and 30% of SCS are used as the primary raw materials, and the FGD is used as the activator to prepare unburned bricks by static pressure forming. The mechanical properties of the specimens at different curing ages were tested by compressive strength test. The hydration mechanism and microstructure of unburned brick were investigated by X-ray diffraction (XRD), scanning electron microscopy (SEM), energy dispersive spectrometer (EDS), thermogravimetric (TG), Fourier transform infrared spectroscopy (FTIR), and inductively coupled plasma-optical emission spectrometry (ICP-OES). The results show that the compressive strength of the specimen increases first and then decreases with the increase of FGD content, and the compressive strength reaches the maximum when the FGD content is 5%. The microscopic test results show that the presence of FGD promoted a higher degree of CFA and SCS dissolution, increasing ettringite formation, which is responsible for strength increase, but extreme doses of FGD resulted in strength degradation. Meanwhile, the higher $\text{SiO}_2/\text{Al}_2\text{O}_3$ ratio confirms the simultaneous formation of hydrated calcium silicate (C-S-H) gel and hydrated calcium aluminosilicate (C-A-S-H) gel within the hydrated product, while a low $\text{SiO}_2/\text{Al}_2\text{O}_3$ ratio confirms the simultaneous formation of ettringite.

Keywords: circulating fluidized bed fly ash; silicon-calcium slag; desulfurization gypsum; unburned brick



Citation: Zhang, L.; Guo, L.; Zhao, Y.; Li, M. Properties of Unburned Brick Produced by Entirely Waste-Stream Binder Activated by Desulfurization Gypsum. *Metals* **2022**, *12*, 2130. <https://doi.org/10.3390/met12122130>

Academic Editor: Jean François Blais

Received: 16 November 2022

Accepted: 8 December 2022

Published: 11 December 2022

Publisher's Note: MDPI stays neutral with regard to jurisdictional claims in published maps and institutional affiliations.



Copyright: © 2022 by the authors. Licensee MDPI, Basel, Switzerland. This article is an open access article distributed under the terms and conditions of the Creative Commons Attribution (CC BY) license (<https://creativecommons.org/licenses/by/4.0/>).

1. Introduction

In the past few decades, due to the rapid industrialization and urbanization in China, the increasing energy consumption is generating a large amount of industrial solid wastes [1,2]. Approximately 60–70 billion tons of industrial solid waste were historically stockpiled in China, and more than 3 billion tons of solid waste were generated annually. These waste materials caused severe problems relating to land occupation, environmental hazards, and social impact [3,4]. Among the industrial solid wastes, 60% consist of fly ash, smelting slag, and desulfurization gypsum [5]. With the rising awareness of sustainable development, China has enhanced the development of green, low-carbon, and circular materials [6] to improve the overall utilization rate of industrial solid waste nationwide.

Unburned brick is an environmentally friendly construction material produced by industrial solid wastes, which is composed of fly ash, tail slag, and smelting slag as primary raw materials, and a small amount of binder or activator. It only requires static pressure forming, curing at room temperature or high temperature without calcination [7]. Compared with traditional sintered clay bricks, unburned bricks have apparent advantages in consuming industrial solid waste, saving clay resources and production energy consumption, reducing carbon and emission, and protecting the environment. At the same time,

unburned bricks have high mechanical strength and excellent durability. They are widely used as masonry bricks, pavement bricks, and dike protection bricks in housing, urban road construction, and river paving, meeting the requirements of sustainable development and broad prospects for growth [8].

Researchers have done much work on preparing unburned bricks from industrial solid waste in recent years. In Mongolia, the Erdenet enterprise uses the industrial waste accumulated by mining enterprises as a new resource base and produces building materials (including bricks made of metal-enriched waste) [9,10]. Poland has also conducted much research on the technical field of developing and utilizing fly ash to produce autoclaved aerated concrete (AAC) [11]. Morsy et al. [12] used straw, ash, soil, and alkaline activator to prepare unburned bricks and tested their compressive strength. Under the dosage of 10% sodium hydroxide and 20% rice straw ash, the maximum compressive strength of the new composite is 2.1 MPa. Wang et al. [13] found that when the mass ratio of tailings: fly ash: cement is 5:2:3, the compressive strength of unburned brick is the best, and its compressive strength reaches 26 MPa after 28 days of curing. As the main reaction product, C-S-H gel produced in the curing process is beneficial in improving the strength of unburned bricks. Liu et al. [14] prepared unburned permeable bricks from metallurgical solid wastes such as steel slag and slag. The prepared brick has the advantages of a high utilization rate of solid waste (96%), excellent performance, and no secondary pollution to the environment. The optimum mixing recipe consists of 20% steel slag, 41% blast furnace slag, 10% fly ash, 15% cement, 12% desulfurized gypsum, and 2% lime. After 28 days of curing, the compressive strength of the matrix is 27.4 MPa. When the blast furnace slag is replaced by steel slag from 20% to 40%, the 28 day compressive strength increases by 5 MPa for every 10% increase of steel slag. However, when the blast furnace slag was replaced by fly ash from 15% to 35%, the 28 day compressive strength decreased by around 4 MPa for every 5% increase in fly ash. The toxicity leaching test shows that the ecological incombustible permeable brick is an environmentally friendly product. Sadique M [15] developed a new composite cementitious material by grinding and blending high calcium fly ash (FA1) and alkali sulfate-rich fly ash (FA2) with amorphous silica fume with FGD as a grinding aid. In this research, FGD is limited as a grinding aid and contributes sulfate ions during the hydration reaction; FA1 and FA2 provide a substantial Ca, Al, K, and Si composition with high pH C-K-S-H gel as the main hydrates. When 60% FA1, 20% FA2, and 20% silica fume is used as a ternary blend, the 28 day compressive strength of the ternary blend increases 27.8% from the strength of the FA with 5% desulfurization gypsum assisted ground. Rust et al. [16] also used two kinds of fly ash and FGD to formulate low-energy cement products. In this system, class F fly ash contains 54.34% SiO₂, which can provide a substantial composition of Si. Chen et al. [17] investigated that CFA of no-cement SFC binder (mixture of GGBFS, class F fly ash, and CFA) had the same effect as FGD of a new composite cementitious material and also contributed sulfate ion during the hydration reaction. GGBFS provides sufficient alkalis and releases heat, which plays a crucial role in the pozzolanic reaction to produce ettringite and C-A-S-H gel. When SFC binder content is 15–20%, CFBC fly ash has the highest compressive strengths for fixed FA.

In conclusion, alkali, salt, and other substances have been used to stimulate industrial solid waste with specific activities to prepare unburned brick has become a research hotspot in recent years. However, it should be pointed out that the previous research mainly focused on the preparation of unburned brick products and the test of macro mechanical properties, and the research depth on hydration characteristics and strength development mechanism of the unburned brick was insufficient. Hence, a comprehensive understanding of the hydration and hardening mechanism of raw materials under the specific cementitious system will be beneficial towards a relatively perfect theoretical support for the preparation of unburned brick.

In this paper, 70% of CFA and 30% of SCS are used as the primary raw materials, and the FGD is used as the activator to prepare unburned bricks by static pressure forming. Among them, SCS is a kind of by-product generated from the extracting aluminum from

fly ash process consisting of lots of CaO, which provides high alkali for hydration. The FGD provides sulfate ion during the hydration to depolymerize the density glass structure of CFA and facilitates further penetration of Ca^{2+} . The effects of different amounts of FGD on the mechanical properties of unburned bricks were studied. At the same time, the hydration and hardening characteristics of the composite cementitious system were analyzed using XRD, SEM, TG, FTIR, and ICP-OES.

2. Materials and Methods

2.1. Raw Materials

The circulating fluidized bed fly ash (CFA) is grayish-black, as shown in Figure 1a. It is generated from the combustion of coal gangue with a specific surface area of $14.857 \text{ m}^2/\text{g}$. Desulfurization gypsum (FGD) is light yellow, as shown in Figure 1b. It is a by-product of flue gas desulfurization in the power plant. Silica-calcium slag (SCS) is a kind of industrial solid waste produced by extracting aluminum from high alumina fly ash and is grayish-white, as shown in Figure 1c. The unburned brick sample after pressure molding is shown in Figure 2. The chemical compositions of raw materials are shown in Table 1, which was determined by an x-ray fluorescence spectrometer (Axios, Panalytical, Netherlands). Additionally, its mineral phases which were measured by XRD analysis using a D600 diffractometer (Cu Ka, 40 kV, 40 Ma), are given in Figure 3. The particle size distribution, estimated by a laser particle size analyzer (MS2000, Malvern, England), is shown in Figure 4, where the CFA particle is significantly smaller than others to improve the pozzolanic reaction activity.

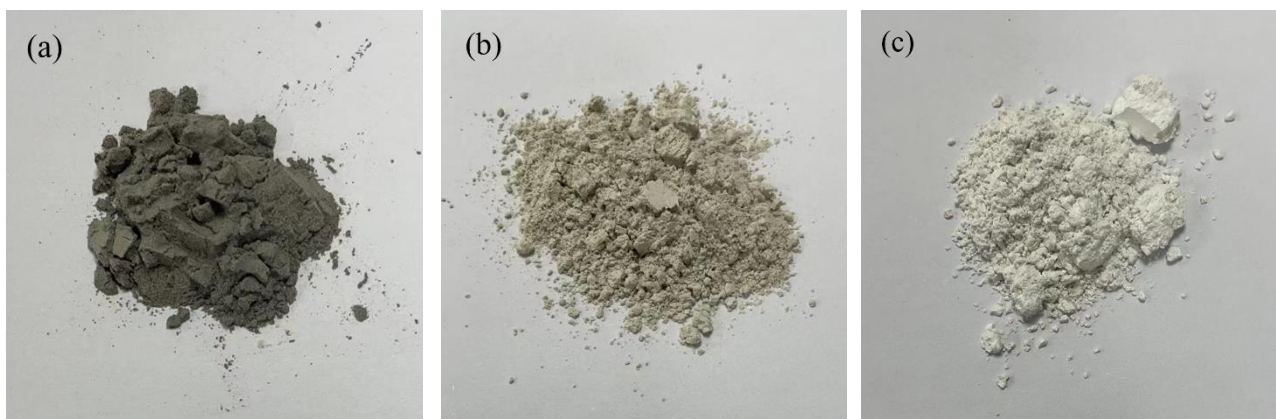


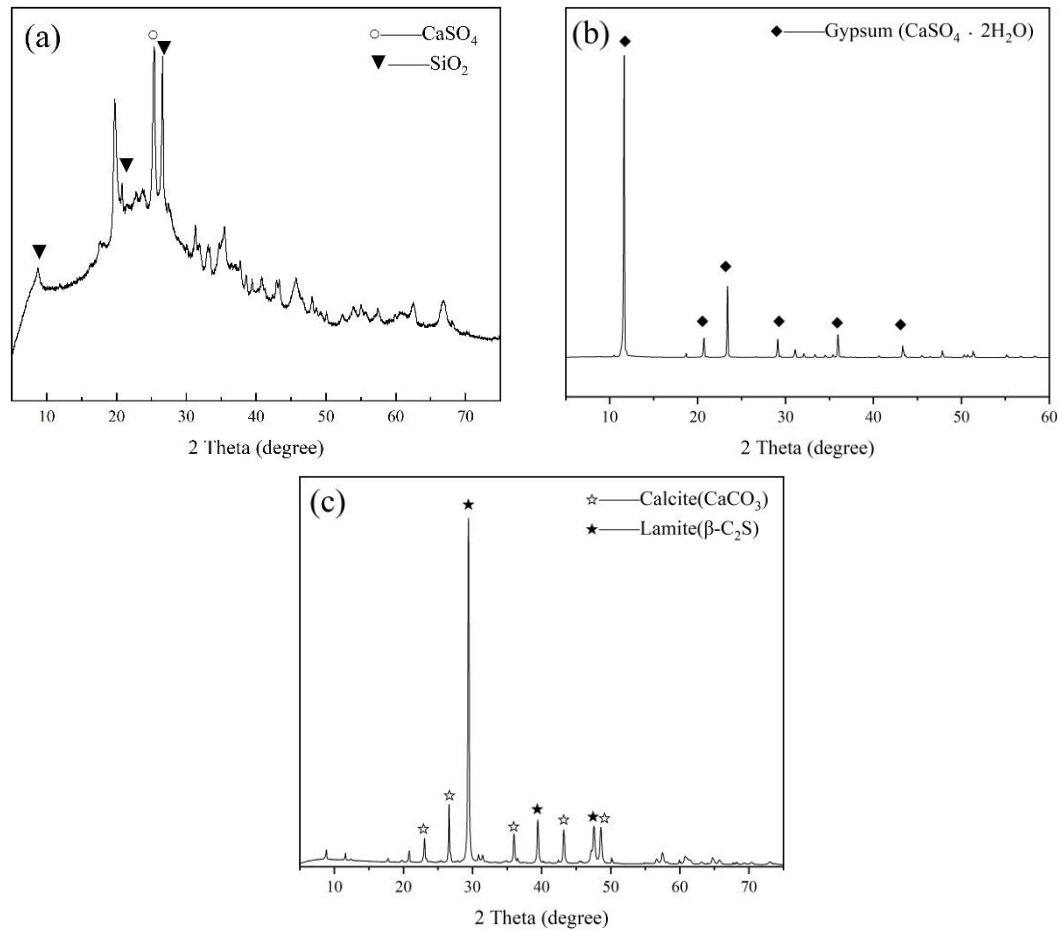
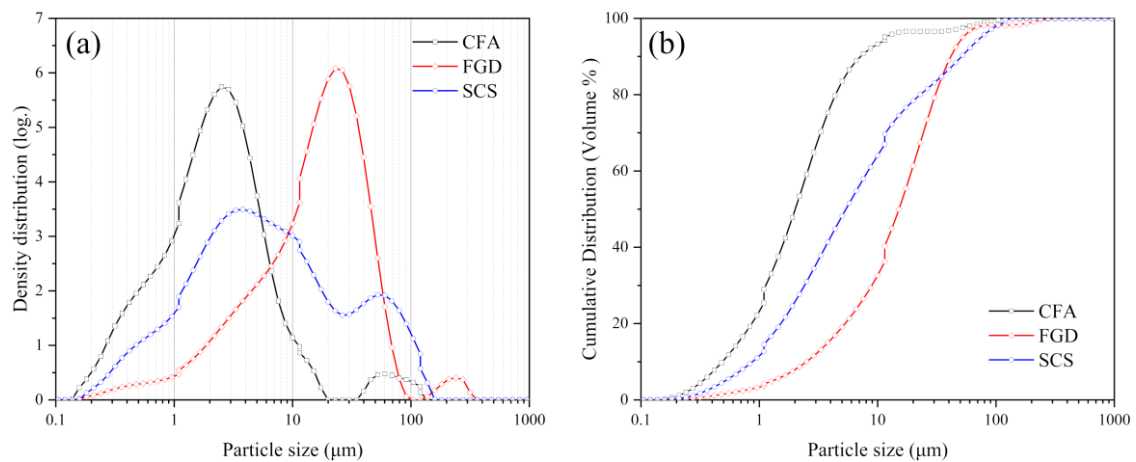
Figure 1. Photos of raw materials: (a) CFA; (b) FGD; and (c) SCS.



Figure 2. Sample of unburned brick.

Table 1. Chemical compositions of raw materials (wt.%).

Materials Types (wt.%)	CaO	SiO ₂	Al ₂ O ₃	Fe ₂ O ₃	MgO	SO ₃	K ₂ O	Na ₂ O	L.O.I
CFA	3.31	36.16	40.53	2.53	1.43	0.88	0.86	0.46	13.84
FGD	36.52	3.26	2.03	0.39	0.74	49.22	0.33	0.33	7.18
SCS	42.46	10.64	3.04	1.63	1.04	0.59	0.60	-	24.00

**Figure 3.** Phases identified by XRD method in examined samples: (a) CFA; (b) FGD; and (c) SCS.**Figure 4.** (a) The cumulative grain size distribution and (b) differential grain size distribution of raw materials.

2.2. Specimens Preparation

The mixture proportions are shown in Table 2. This research was based on a new cementitious agent consisting of 70% of CFA and 30% of SCS. FGD was an activator chemical in this study. The specimens were prepared as follows. CFA, SCS, and FGD were mixed and stirred. The water-to-binder ratio is 0.2. The pastes were prepared by the method of compression molding under 20 MPa. The unburned bricks began to be cured in a steamer at 60 °C for about 24 h. When the unburned bricks were cured at a temperature of about 20 ± 1 °C and >95% relative humidity to testing ages, the middle portions of specimens were obtained, broken, and soaked in absolute ethanol to stop hydration.

Table 2. Mixture proportions of paste samples.

Binder	CFA/(wt.%)	SCS/(wt.%)	FGD/(wt.%)	Molding Pressure/(MPa)	Thermal/(°C)
FCG-1	70	30	1	20	60
FCG-2	70	30	3		
FCG-3	70	30	5		
FCG-4	70	30	8		
FCG-5	70	30	10		

2.3. Compressive Strength Test

Compressive strength is tested by a CS200 universal strength testing apparatus (50 KN capacity, Weiheng, Ningbo, China). Three specimens were tested each time for each exposure. The average value of the three tested specimens was presented. The strength loading rate and fine strength are calculated according to the China standard GB/T 5486–2008.

2.4. Microscopic Tests

2.4.1. XRD

X-ray diffractometer (XRD) uses Ultima-IVX-Ra (Rigaku, Tokyo, Japan) (Cu K α radiation, 40 kV, 40 Ma, 0.02° 2 θ step-scan and 10 s per step) for crystalline phase. The samples are tested from 5 to 60 with a 5°/min speed.

2.4.2. SEM

Scanning electron microscope (SEM) is tested by JSM-6700F (JEOL, Tokyo, Japan), which is used to observe the micromorphology of products. It is combined with an energy dispersive spectrometer (EDAX, Mahwah, NJ, USA) to analyze the hydration products.

2.4.3. TG

Thermogravimetry (TG) measurement is tested by Q600 SDT (TA, Milford, CT, USA), which is used to test the number of hydration products. The samples are tested from room temperature to 800 °C with a heating rate of 20 °C/min in a nitrogen atmosphere.

2.4.4. FTIR

Fourier transform infrared spectroscopy (FTIR) is tested by a PE1750 (PerkinElmer, Waltham, MA, USA). The samples are tested from 400 to 4000 cm^{−1}. It is used to estimate the amorphous product of hydration.

2.4.5. ICP-OES

ICP-OES is tested by Agilent 5110 (Agilent, Palo Alto, CA, USA). The concentration of Ca, Si, and Al were measured. The elements were chosen because they are the three most frequent elements in the tested binders.

3. Results and Discussion

3.1. Compressive Strength

Compressive strength is one of the major indexes used to evaluate the mechanical performance of unburned brick. Figure 5 shows the effect of FGD on the compressive strength of the unburned brick made by the FCG binder. The results prove that the compressive strength of specimens increased with FGD content from 1% to 5%. Specifically, after 28 days of curing, the compressive strength of specimens FCG-1, FCG-2, and FCG-3 are 4.82 MPa, 5.01 MPa, and 6.06 MPa, respectively. Compared with FCG-1, the compressive strength of specimens FCG-2 and FCG-3 increased by 3.94% and 25.73%, respectively. The improved compressive strength of unburned brick was mainly due to the pozzolanic reaction of CFA and SCS particles activated by the penetrating sulfate ions from FGD. More hydration products will be formed, leading to the denser microstructures of specimens and higher strength. However, when the FGD content exceeds 5%, the compressive strength of specimens FCG-4 and FCG-5 after curing for 28 days is 5.66 MPa and 5.41 MPa, and decreases by 6.61% and 10.73%, respectively, compared with FCG-3, but it is still higher than that of specimen FCG-1 by 4.83 MPa. It shows that the optimum content of FGD is 5%, and when the addition of FGD is more than 5%, due to 5% FGD was enough to activate CFA and LAFA, but excess FGD was harmful to strength because of its nonhydraulic, the compressive strength started to decline.

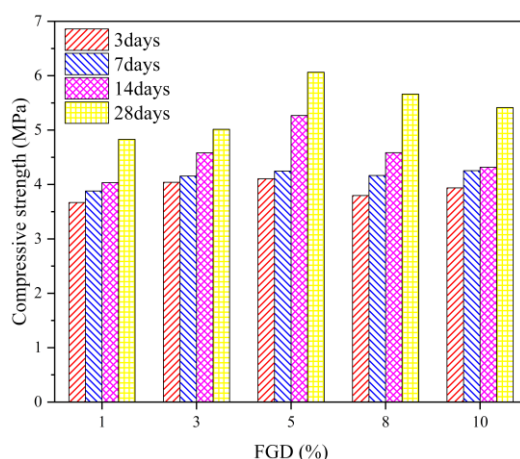


Figure 5. Compressive strength of brick with binary blends.

The compressive strength of specimen FCG-3 cured for 3 days, 7 days, 14 days, and 28 days is 4.11 MPa, 4.25 MPa, 5.27 MPa, and 6.06 MPa, respectively. Given that the FGD addition produced a significant strength improvement after 7 days, the use of FGD would significantly affect the later reaction after 7 days. At the same time, it can be seen that the compressive strength of the specimen is generally low, and the highest compressive strength is 6.06 MPa when the content of FGD is 5% at 28 days. Early studies [18,19] show that $\text{Ca}(\text{OH})_2$ produced by cement hydration destroys the dense crystal structure in the mineral additions, resulting in the pozzolanic activity of the mineral additions material being excited and secondary hydration. However, in the no-cement FFG binder, the system's alkalinity is generally low. The mineral additions need more time to destroy the dense crystal structure, resulting in a prolonged early hydration rate, so the effect of FGD on the compressive strength is minimal.

3.2. Effect of FGD Content on Hydration Product

3.2.1. XRD

Figure 6 presents the effect of FGD on the phase changes of unburned bricks at 28 days. It is worth noting that ettringite is one of the significant hydration products. The amount of ettringite increased with the rise of FGD due to the charging of sulfate ion contributed by

FGD. The formulating of ettringite contributed to the engineering properties. However, when the FGD content exceeds 5%, the diffraction peak of gypsum appears in the hydration product, and the diffraction peak increases significantly with the increase of FGD content. The results show that only part of sulfate ions in FGD dissolve and react to form ettringite, and the remaining unreacted parts still exist in the form of gypsum, which only plays the role of filler in the system, increases the porosity of the system, and finally reduces the compressive strength of the specimen.

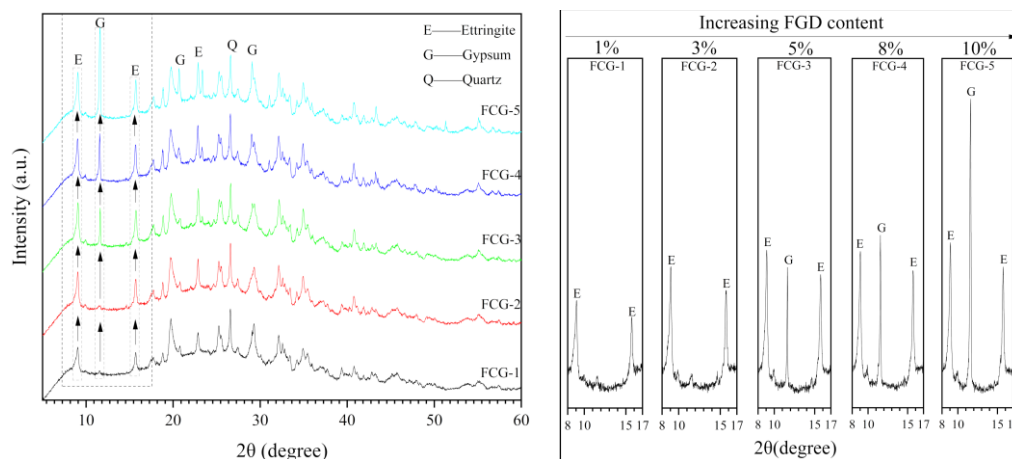


Figure 6. XRD patterns of FCG pastes for different FGD in 28 days.

Figure 7 shows the progressive formation of these hydration products and the unreacted reactants by XRD analysis. The peaks of ettringite are stable but slightly rising until 7 days, which shows similar trends to the compressive strength. Similar conditions are to be found, showing that the reflections of gypsum had no apparent changes in the peak intensity, which reflects the low reaction rate of pozzolanic reaction. At the later ages of 14 and 28 days, the peak of ettringite has a significant change, which means that further hydration produced more ettringite. The peaks of gypsum were the complete opposite of ettringite. The results of XRD are coincident with the compressive strength presented in Figure 3. According to the previous study [20,21], the broad hump around 15° – 40° was the characteristic of amorphous SiO_2 and gels. In Figure 5, the broad hump around 15 – 40° is significant, while the X-ray amorphous nature of the gels makes it unidentifiable by XRD.

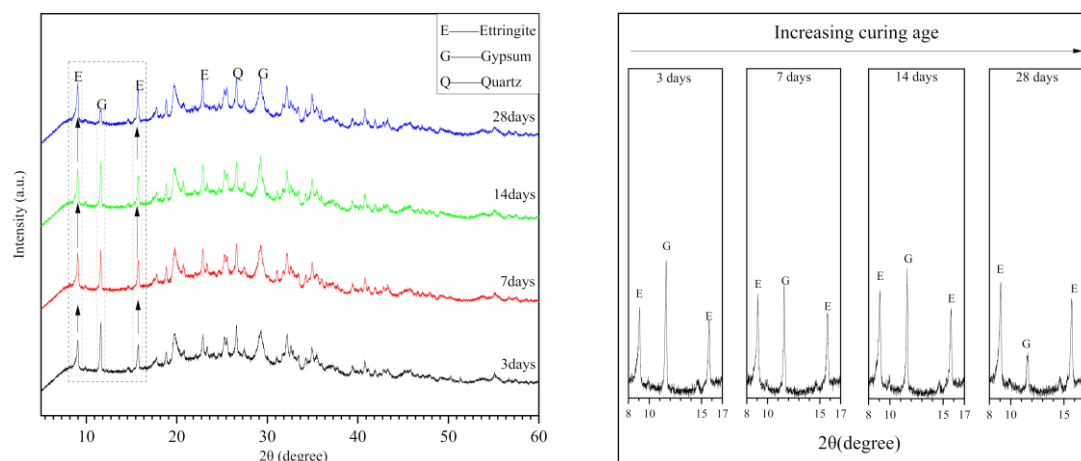


Figure 7. XRD patterns of FCG paste for 5% FGD at different curing ages.

3.2.2. SEM-EDS

The internal morphology of FCG-1 and FCG-3 specimens cured for 28 days were observed by SEM, and the chemical components of FCG-3 were analyzed by EDS, as shown in Figure 8. As can be seen from the images, a considerable number of needle-rod reaction products (as shown in Figure 8b) have occurred in the sample FCG-3, and EDS analysis indicates that the main elements of the substance are Ca, S, O, Al, and Si (as shown in Figure 8c). Based on the morphology and elemental composition of the reaction product, the substance is ettringite, further confirming the analysis result of XRD in Figure 6. Figure 8a shows that some fibrous C-S-H gels are formed in the specimen FCG-1 and that there are relatively few internal needle rod reaction products, which is related to the low content of FGD. At the same time, it further shows that the addition of FGD is conducive to the formation of ettringite [22].

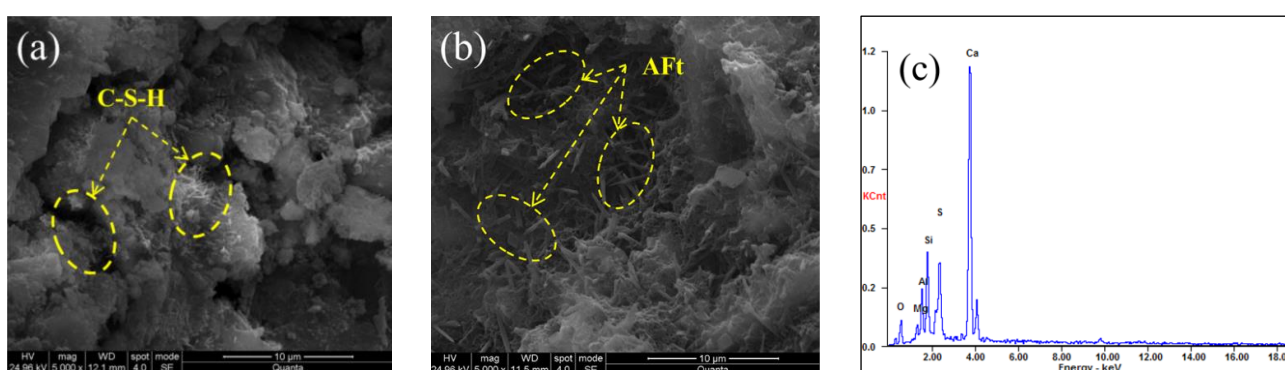


Figure 8. SEM patterns of FCG pastes for different FGD in 28 days: (a) FCG-1; (b) FCG-3; and (c) EDS of FCG-3.

3.2.3. TG

The TG and heat flow results at 28 days are present in Figure 9. Several distinct loss stages, named I and II, are present at temperatures between 60 °C and 170 °C, likely due to the decomposition of ettringite, gels, and gypsum [23,24]. The weight loss increased as the addition of FGD increased from 1% to 5% at stage I primarily. When the addition of FGD is more than 5%, the weight loss mainly increases at stage II, consistent with gypsum decomposition. The weight loss at stage II is mainly associated with the decomposition of ettringite and gels. TG analysis provides that the hydration product is increased as the addition of FGD increases, and when the addition of FGD is more than 5%, the hydration product emerges in unreacted gypsum, which is consistent with the X-ray diffraction results.

In cementitious systems, the total loss of mass between room temperature and 600 °C can estimate the degree of hydration [25]. Figure 9b presents the total mass loss between room temperature and 600 °C. The weight losses were quite similar among the samples containing FGD, even though the weight loss slightly increased with increasing FGD content, reflecting the improvement of the degree of hydration. However, the weight loss slightly decreased because of the FGD containing more than 5%.

The TG and heat flow results of FCG-3 at different ages are present in Figure 10. At stage I, the weight loss has no significant changes until 7 days, which mainly increased between 7 days and 28 days. The weight loss at stage II has an opposite trend, which proved the formation of ettringite and gels. It is consistent with the result of XRD. Figure 10b presents the total mass loss between room temperature and 600 °C, consistent with the weight loss at stage I.

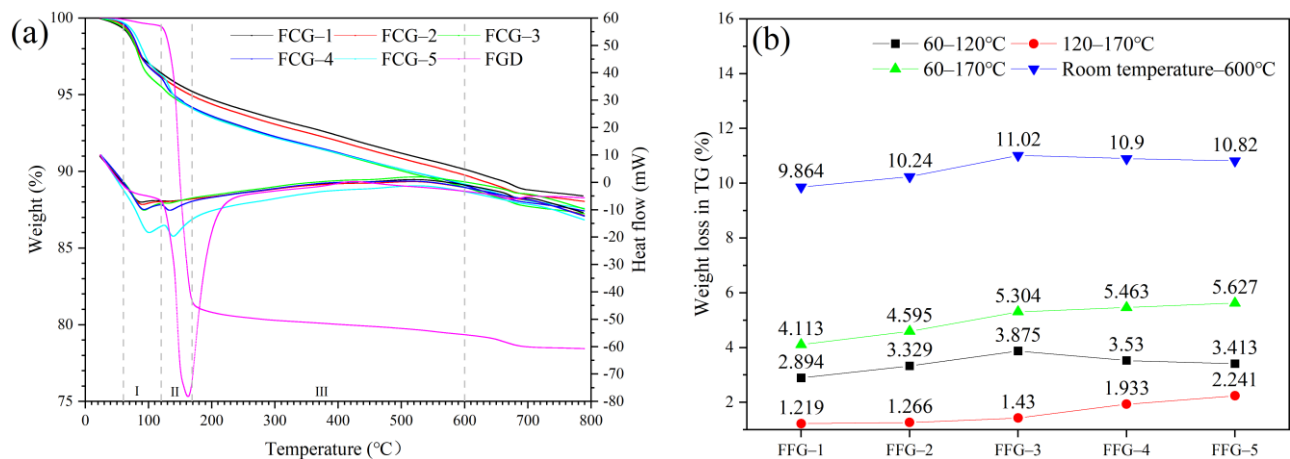


Figure 9. (a) TG and heat flow of bricks at 28 days; (b) the weight loss of TG at different stages.

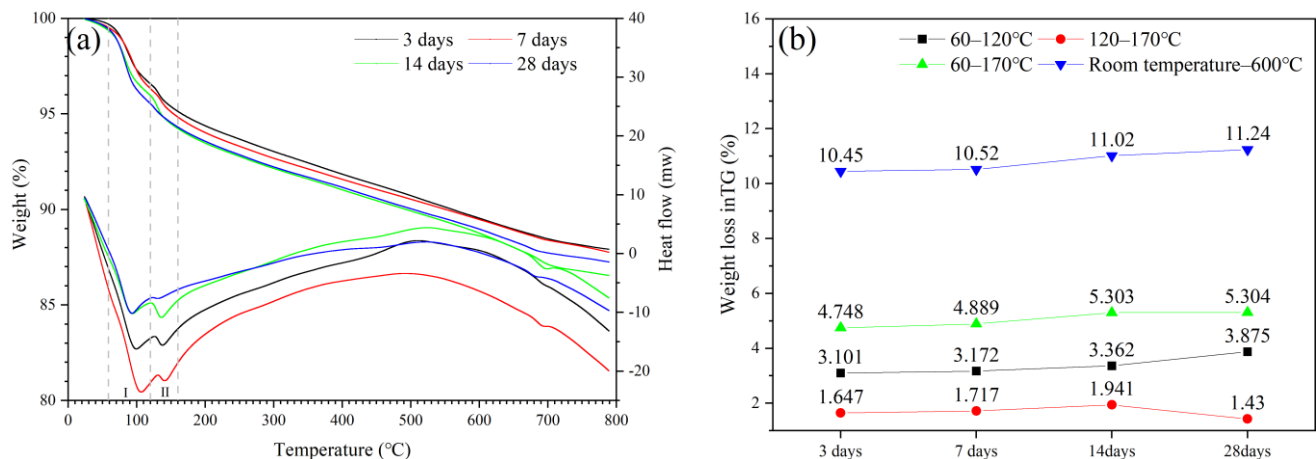


Figure 10. (a) TG and heat flow of FCG-3 at different ages; (b) the weight loss of TG at different stages.

3.2.4. FTIR

Figure 11a shows the FTIR spectra for the different mixtures at 28 days. The broad bands located between 3350 cm^{-1} and 3450 cm^{-1} in the spectra correspond to the tension and bending vibrations of the fundamental O-H bond in the water [26]. The broad bands located between 1050 and 1100 cm^{-1} in the spectra correspond to the Si-O-Si bond of the produced gels [27,28]. With an increasing FGD content, the reflections of gels were changed sharper, which indicates that the polymerization of the Si-O bond increases [29]. Figure 11b shows that as the reaction proceeds, the peak width gradually narrows and becomes sharper, indicating that the polymerization of the Si-O bond increases with the increase of age.

3.2.5. ICP-OES

In order to explore the controlling factors of the no-cement binders, the concentration of the extraction solution, such as aluminum (Al), calcium (Ca), and silica (Si), is investigated, as shown in Figure 12. The results show that the concentration of dissolved Ca and Si are higher when the FGD dosage is higher. The increase in Ca and Si concentrations are expected to be due to the enhanced dissolution of CFA and SCS. The results explain the increased compressive strength with increasing FGD dosage, as shown in Figure 3.

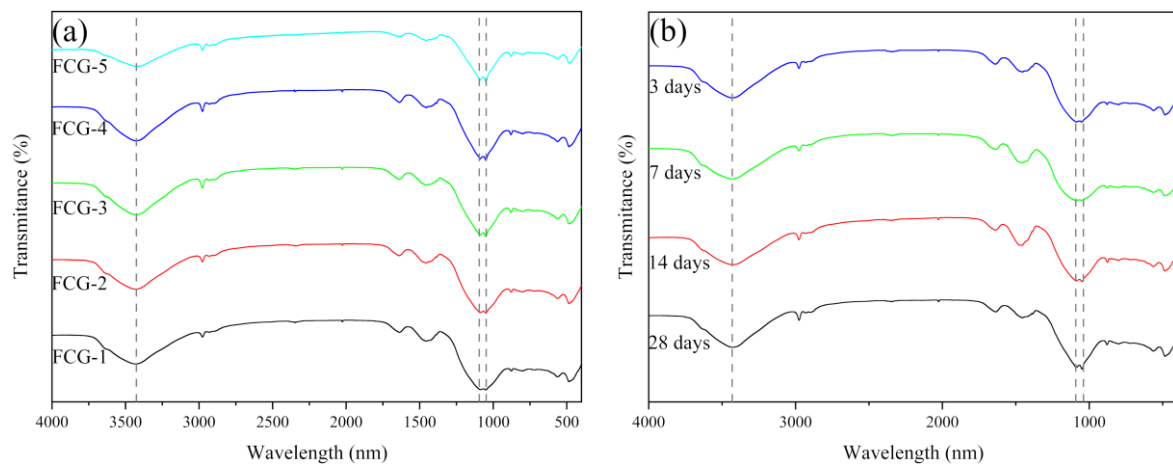


Figure 11. FTIR spectra of (a) bricks with different compositions in 28 days and (b) bricks with 5% FGD at different ages.

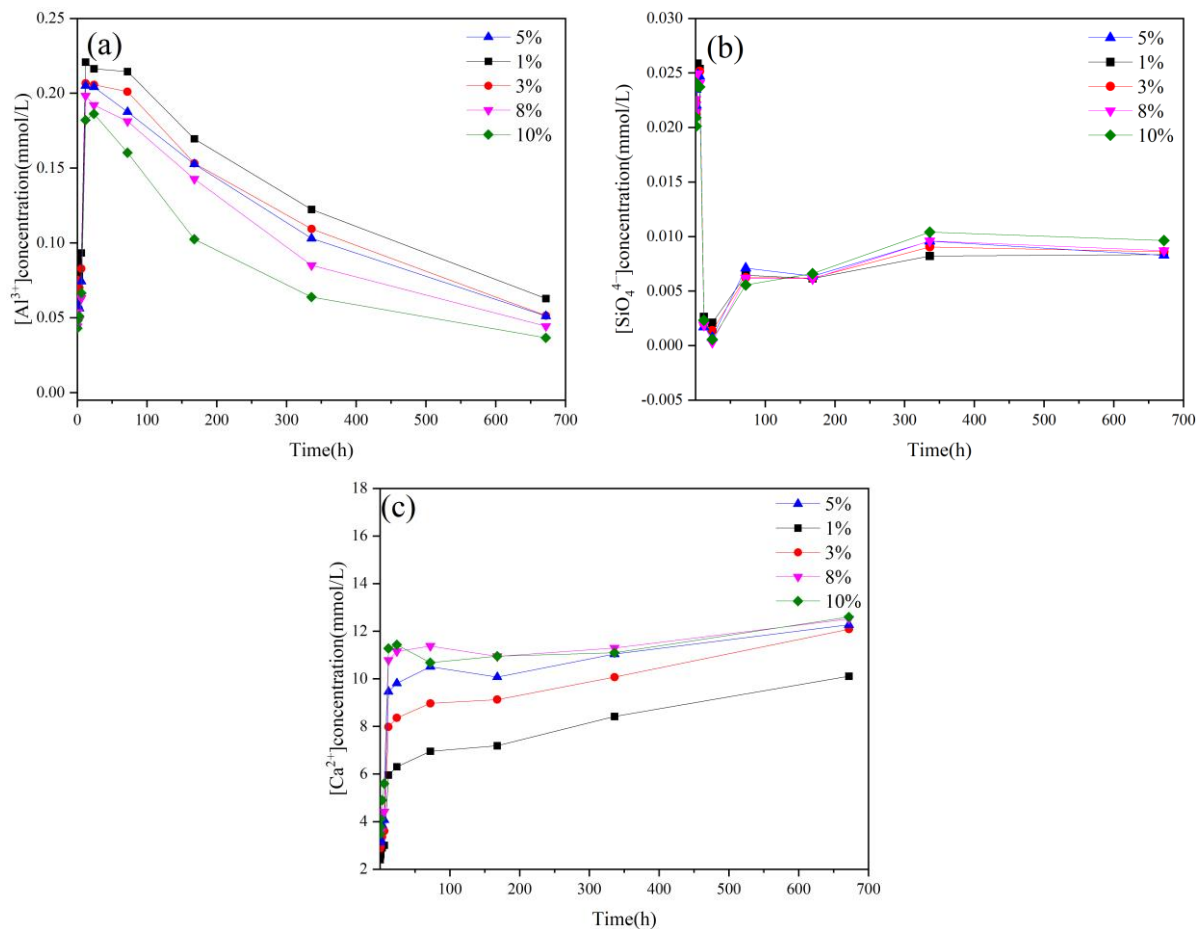


Figure 12. Ionic concentration of binders: (a) Al^{3+} ; (b) SiO_4^{4-} ; and (c) Ca^{2+} .

When the FGD dosage is higher, more than 5%, the concentration of dissolved Ca and Si was similar, even though the concentration increased slightly with increasing FGD content. By contrast, the concentration of dissolved Al decreased significantly, which decreased the formation of gels and ettringite, resulting in the loss of strength (see Figure 5).

Figure 13 illustrates the results of ICP-OES for the binder with 5% FGD at different ages. After 24 h, the Ca, Si, and Al concentrations have a significant change. The evolution

of Ca and Si have the same trend, but the evolution of Al goes by contrast. Many studies show that portlandite is only simulated at low Al content as a function of increasing SiO₂ concentration [30,31]. Figure 13 shows the same trend.

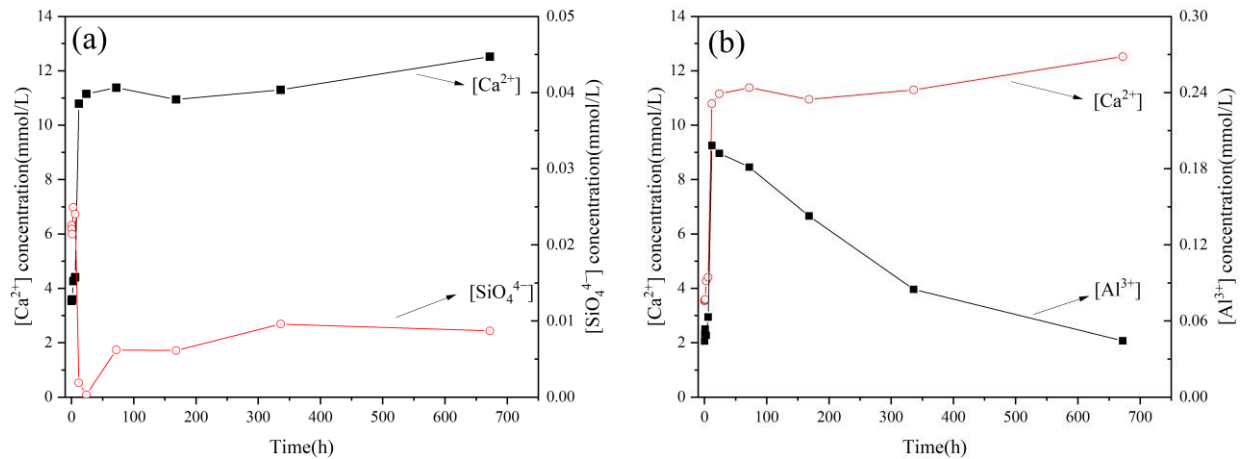


Figure 13. Ionic concentration of FCG-3: (a) Ca^{2+} and SiO_4^{4-} ; (b) Ca^{2+} and Al^{3+} .

3.3. Analysis of the Optimal Mixture

First, the characteristics of these binders are analyzed from the chemical composition of raw materials, as shown in Figure 14. The most prominent feature of these binders is their low calcium content. In these binders, the ratio of CaO/Al₂O₃ is about 1, and the ratio of CaO/SiO₂ is around 0.5. The composition of CaO is lower than in most studies. CaO not only provides an alkaline environment but also participates in forming hydration products. Therefore, from the analysis of the raw materials, low CaO content is the critical factor limiting strength development and the formation of hydration products.

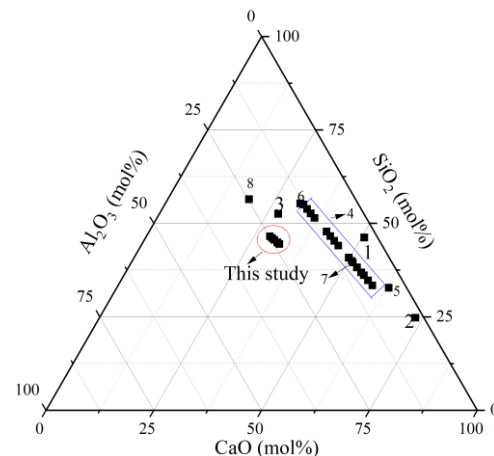
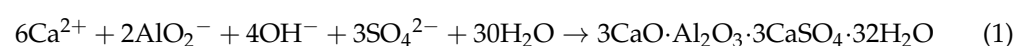
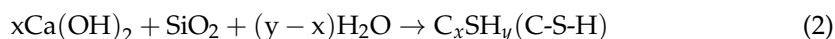


Figure 14. Ternary phase diagram of the binders (1 [15] 2 [32] 3 [33] 4 [17] 5 [34] 6 [35] 7 [36] 8 [37]).

In order to improve the compressive strength of unburned bricks made of FCG binder, the formation of ettringite and gel should be maximized. The ettringite and gels formation in the unburned brick are associated with the chemical composition of binders. Alumina and silica have potential activation in CFA or SCS, where OH[−] activates them to form AlO₂[−] and SiO₄^{4−}. Then, AlO₂[−] reacts with SiO₄^{4−}, Ca²⁺ in the environment to form ettringite, and the SiO₄^{4−} reacts with Ca²⁺ in the environment to form C-S-H gels. The reaction equations may be as follows [38].





However, the silica could be substituted by the reactive aluminum to form C-A-S-H gels [39,40], especially after 7 days [41]. The hydration product was determined by CaO/SiO_2 molar and $\text{SiO}_2/\text{Al}_2\text{O}_3$ ratios. It is reported [42] that a higher $\text{SiO}_2/\text{Al}_2\text{O}_3$ ratio confirms the simultaneous formation of C-S-H gel and C-A-S-H gel within the hydrated product, but a lower $\text{SiO}_2/\text{Al}_2\text{O}_3$ ratio confirms the simultaneous formation of ettringite. In Figure 12, owing to a low CaO/SiO_2 molar ratio at early ages, the hydration rates of blends were lower, which could not generate compressive strength higher [15]. It is consistent with Figure 5. Moreover, a low $\text{SiO}_2/\text{Al}_2\text{O}_3$ ratio confirms the simultaneous formation of ettringite, as shown in Figure 10. Afterward, owing to a simulation at low Al content as a function of increasing SiO_2 concentration, the formation of ettringite consumes some AlO_2^- , leading to a high $\text{SiO}_2/\text{Al}_2\text{O}_3$ ratio, which confirms the simultaneous formation of C-S-H gels and C-A-S-H gels as Figure 10.

The increased FGD induced a high concentration of sulfate ion, which contributed to ettringite formation. However, the dissolution of SCS and CFA did not provide enough dissolved silica and calcium oxide ion to react with the alumina, so the C-S-H/C-A-S-H gels were less, influencing the compressive strength of unburned brick.

4. Conclusions

This study uses industrial solid wastes such as circulating fluidized bed fly ash, calcium silicate slag, and desulfurization gypsum as raw materials to prepare unburned bricks through a pressure-forming process. The preparation process does not require high-temperature calcination, which can significantly reduce energy consumption and carbon emissions in the production process, the use of these unburned bricks could also promote the resource utilization of industrial solid wastes hence mitigating the environmental issues caused by industrial waste stockpiling. In addition, on the premise that all performance indicators meet the use requirements, it can be used as pedestrian pavement bricks in projects with low strength requirements. Through studying the influence of different desulfurized gypsum content on the mechanical properties of unburned bricks and further using XRD, SEM-EDS, TG, FTIR, and ICP-OES microscopic testing methods to analyze its hydration and hardening mechanisms, the following conclusions are obtained:

(1) During the hydration process, the presence of FGD improved the degree of dissolution for CFA and SCS and the formation of ettringite, hence activating the CFA and SCS. Overall, participation of FGD leads to a strength enhancement for the produced construction material (unburned brick).

(2) With the increase of FGD content, the developed compressive strength of un-burned brick showed a rise and fall trend. Moreover, the amount of hydration products in the system changes obviously, and the crystallinity of the product increases. When the FGD content is too large, the amount of unreacted gypsum increases, resulting in a specific decrease in the compressive strength of the specimen. The optimum dosage of FGD was 5%, the strength of unburned brick reaches the maximum, and its 28 days compressive strength is 6.06 MPa.

(3) The increased FGD induced a high concentration of sulfate ion, which contributed to ettringite formation. However, the dissolution of SCS and CFA did not provide enough dissolved silica and calcium oxide ions to react with the alumina, so the C-S-H/C-A-S-H gels were less, influencing the compressive strength of unburned brick.

The above findings may inspire the composition design of the solid waste unburned brick. However, in this paper, only the desulfurization gypsum is used as an activator to prepare unburned bricks. In future research, other alkaline solid wastes or wastes with other ionic activators could be used to achieve the collaborative application of multiple solid wastes. At the same time, the water absorption, frost resistance, and hardness of unburned bricks could be further studied for the durability of unburned brick.

Author Contributions: Conceptualization, L.Z.; Data curation, Y.Z.; Formal analysis, L.Z.; Funding acquisition, L.G.; Investigation, L.Z.; Methodology, L.Z.; Validation, M.L.; Writing—review and editing, L.G. and Y.Z. All authors will be informed about each step of manuscript processing including submission, revision, revision reminder, etc. via emails from our system or assigned Assistant Editor. All authors have read and agreed to the published version of the manuscript.

Funding: This research was funded by the National key R & D plan project grant number 2021YFE0102 900; funded by the National Natural Science Foundation of China grant number 52274122; funded by the Youth Innovation Fund Project (04-2123), and the Exploration Fund Project (02-2229) of BGRIMM Technology Group.

Data Availability Statement: All data, models, and code generated or used during the study appear in the submitted article.

Conflicts of Interest: The authors declare that they have no known competing financial interests or personal relationships that could have appeared to influence the work reported in this paper.

References

1. Zhao, D.; Zhang, B.; Shen, W.; Wu, M.; Guan, Y.; Wu, J.; Zhang, Z.; Zhu, J. High industrial solid waste road base course binder: Performance regulation, hydration characteristics and practical application. *J. Clean. Prod.* **2021**, *313*, 127879. [\[CrossRef\]](#)
2. Zhang, X.; Zhou, M.; Li, J.; Wei, L.; Dong, Y.; Hou, H.; Wang, Z. Analysis of driving factors on China's industrial solid waste generation: Insights from critical supply chains. *Sci. Total Environ.* **2021**, *775*, 145185. [\[CrossRef\]](#) [\[PubMed\]](#)
3. Nai, C.; Tang, M.; Liu, Y.; Xu, Y.; Dong, L.; Liu, J.; Huang, Q. Potentially contamination and health risk to shallow groundwater caused by closed industrial solid waste landfills: Site reclamation evaluation strategies. *J. Clean. Prod.* **2020**, *286*, 125402. [\[CrossRef\]](#)
4. Protano, G.; Baroni, D.; Bianchi, S.; Russo, C.; Salleolini, M. Assessing the impact on groundwater chemistry of an environmental restoration performed using industrial solid waste from TiO₂ production. *Appl. Geochem.* **2020**, *120*, 104666. [\[CrossRef\]](#)
5. Guo, W.; Xi, B.; Huang, C.; Li, J.; Tang, Z.; Li, W.; Ma, C.; Wu, W. Solid waste management in China: Policy and driving factors in 2004–2019. *Resour. Conserv. Recycl.* **2021**, *173*, 105727. [\[CrossRef\]](#)
6. Tang, J.; Wang, Q.; Choi, G. Efficiency assessment of industrial solid waste generation and treatment processes with carry-over in China. *Sci. Total Environ.* **2020**, *726*, 138274. [\[CrossRef\]](#) [\[PubMed\]](#)
7. Zhao, Y.; Liang, N.; Chen, H.; Li, Y. Preparation and properties of sintering red mud unburned road brick using orthogonal experiments. *Constr. Build. Mater.* **2020**, *238*, 117739. [\[CrossRef\]](#)
8. Chindaprasirt, P.; Pimraksa, K. A study of fly ash–lime granule unfired brick. *Powder Technol.* **2008**, *182*, 33–41. [\[CrossRef\]](#)
9. Nyamdorj, D.; Laikhansuren, B.; Davaakhuu, N.; Potravny, I.M. Blasting waste recycling at mines in Mongolia. *Gorn. Zhurnal* **2022**, *3*, 38–42. [\[CrossRef\]](#)
10. Davaakhuu, N.; Potravny, I.M.; Tishkov, S.V.; Kulakov, K.A. Modeling mining company activities under conditions of resource base depletion: Ecological and economic aspect. *Gorn. Zhurnal/Min. J.* **2019**, *8*, 50–54. [\[CrossRef\]](#)
11. Zapotoczna-Sytek, G. AAC of fly ash in the strategy of sustainable development. *Cem. Lime Concr.* **2006**, *3*, 193–201.
12. Morsy, M.I.; Alakeel, K.A.; Ahmed, A.E.; Abbas, A.M.; Omara, A.I.; Abdelsalam, N.R.; Emaish, H.H. Recycling rice straw ash to produce low thermal conductivity and moisture-resistant geopolymer adobe bricks. *Saudi J. Biol. Sci.* **2022**, *29*, 3759–3771. [\[CrossRef\]](#) [\[PubMed\]](#)
13. Wang, W.; Gan, Y.; Kang, X. Synthesis and Characterization of Sustainable Eco-friendly Unburned Bricks from Slate Tailings. *J. Mater. Res. Technol.* **2021**, *14*, 1697–1708. [\[CrossRef\]](#)
14. Liu, L.; Cheng, X.; Miao, X.; Shi, Y.; Zhang, M.; Guo, M.; Cheng, F.; Zhang, M. Preparation and characterization of majority solid waste based eco-unburned permeable bricks. *Constr. Build. Mater.* **2020**, *259*, 120400. [\[CrossRef\]](#)
15. Sadique, M.; Al Nageim, H.; Atherton, W.; Seton, L.; Dempster, N. A new composite cementitious material for construction. *Constr. Build. Mater.* **2012**, *35*, 846–855. [\[CrossRef\]](#)
16. Rust, D.; Rathbone, R.; Mahboub, K.C.; Robl, T. Formulating Low-Energy Cement Products. *J. Mater. Civ. Eng.* **2012**, *24*, 1125–1131. [\[CrossRef\]](#)
17. Chen, C.T.; Nguyen, H.A.; Chang, T.P.; Yang, T.R.; Nguyen, T.D. Performance and microstructural examination on composition of hardened paste with no-cement SFC binder. *Constr. Build. Mater.* **2015**, *76*, 264–272. [\[CrossRef\]](#)
18. Makhloufi, Z.; Kadri, E.H.; Bouhicha, M.; Benaissa, A.; Bennacer, R. The strength of limestone mortars with quaternary binders: Leaching effect by demineralized water. *Constr. Build. Mater.* **2012**, *36*, 171–181. [\[CrossRef\]](#)
19. Makhloufi, Z.; Bederina, M.; Bouhicha, M.; Kadri, E.-H. Effect of Mineral Admixtures on Resistance to Sulfuric Acid Solution of Mortars with Quaternary Binders. *Phys. Procedia* **2014**, *55*, 329–335. [\[CrossRef\]](#)
20. Taylor, H.F.W. *Cement Chemistry*, 2nd ed.; Thomas Telford: London, UK, 1997.
21. Wang, S.D.; Scrivener, K.L. Hydration products of alkali activated slag cement. *Cem. Concr. Res.* **1995**, *25*, 561–571. [\[CrossRef\]](#)
22. Jebli, M.; Jamin, F.; Pelissou, C.; Lhopital, E.; El Youssoufi, M. Characterization of the expansion due to the delayed ettringite formation at the cement paste-aggregate interface. *Constr. Build. Mater.* **2021**, *289*, 122979. [\[CrossRef\]](#)

23. Vedalakshmi, R.; Raj, A.S.; Srinivasan, S.; Babu, K.G. Quantification of hydrated cement products of blended cements in low and medium strength concrete using TG and DTA technique. *Thermochim. Acta* **2003**, *407*, 49–60. [\[CrossRef\]](#)
24. Ubbriaco, P.; Calabrese, D. Solidification and stabilization of cement paste containing fly ash from municipal solid waste. *Thermochim. Acta* **1998**, *321*, 143–150. [\[CrossRef\]](#)
25. Angulo-Ramírez, D.E.; Gutiérrez, R.M.D.; Puertas, F. Alkali-activated Portland blast-furnace slag cement: Mechanical properties and hydration. *Constr. Build. Mater.* **2017**, *140*, 119–128. [\[CrossRef\]](#)
26. Manso, S.; Mestres, G.; Ginebra, M.-P.; De Belie, N.; Segura, I.; Aguado, A. Development of a low pH cementitious material to enlarge bioreceptivity. *Constr. Build. Mater.* **2014**, *54*, 485–495. [\[CrossRef\]](#)
27. Puertas, F.; Palacios, M.; Manzano, H.; Dolado, J.S.; Rico, A.; Rodríguez, J. A model for the C-A-S-H gel formed in alkali-activated slag cements. *J. Eur. Ceram. Soc.* **2011**, *31*, 2043–2056. [\[CrossRef\]](#)
28. García-Lodeiro, I.; Palomo, A.; Fernández-Jiménez, A.; Macphee, D.E. Compatibility studies between N-A-S-H and C-A-S-H gels. Study in the ternary diagram $\text{Na}_2\text{O}-\text{CaO}-\text{Al}_2\text{O}_3-\text{SiO}_2-\text{H}_2\text{O}$. *Cem. Concr. Res.* **2011**, *41*, 923–931. [\[CrossRef\]](#)
29. Dakhane, A.; Tweedley, S.; Kailas, S.; Marzke, R.; Neithalath, N. Mechanical and microstructural characterization of alkali sulfate activated high volume fly ash binders. *Mater. Des.* **2017**, *122*, 236–246. [\[CrossRef\]](#)
30. Shi, Z.; Shi, C.; Wan, S.; Ou, Z. Effect of alkali dosage on alkali-silica reaction in sodium hydroxide activated slag mortars. *Constr. Build. Mater.* **2017**, *143*, 16–23. [\[CrossRef\]](#)
31. Iler, R.K. Effect of adsorbed alumina on the solubility of amorphous silica in water. *J. Colloid Interface Sci.* **1973**, *43*, 399–408. [\[CrossRef\]](#)
32. Zhao, J.; Wang, D.; Yan, P.; Zhang, D.; Wang, H. Self-cementitious property of steel slag powder blended with gypsum. *Constr. Build. Mater.* **2016**, *113*, 835–842. [\[CrossRef\]](#)
33. Zhong, S.; Ni, K.; Li, J. Properties of mortars made by uncalcined FGD gypsum-fly ash-ground granulated blast furnace slag composite binder. *Waste Manag.* **2012**, *32*, 1468–1472. [\[CrossRef\]](#) [\[PubMed\]](#)
34. Makhloufi, Z.; Chettih, M.; Bederina, M.; Kadri, E.H.; Bouhicha, M. Effect of quaternary cementitious systems containing limestone, blast furnace slag and natural pozzolan on mechanical behavior of limestone mortars. *Constr. Build. Mater.* **2015**, *95*, 647–657. [\[CrossRef\]](#)
35. Jeon, D.; Yum, W.S.; Jeong, Y.; Oh, J.E. Properties of quicklime (CaO)-activated Class F fly ash with the use of CaCl_2 . *Cem. Concr. Res.* **2018**, *111*, 147–156. [\[CrossRef\]](#)
36. Zhao, J.; Li, D.; Liao, S.; Wang, D.; Wang, H.; Yan, P. Influence of mechanical grinding on pozzolanic characteristics of circulating fluidized bed fly ash (CFA) and resulting consequences on hydration and hardening properties of blended cement. *J. Therm. Anal. Calorim.* **2018**, *132*, 1459–1470. [\[CrossRef\]](#)
37. Shao, N.; Liu, Z.; Fan, J.; Zhou, Y.; Wang, D. Phase evolution of fly ash calcium constituent at early alkali activation reaction age. *Mater. Lett.* **2016**, *174*, 175–179. [\[CrossRef\]](#)
38. Dung, N.T.; Chang, T.P.; Chen, C.T. Engineering and sulfate resistance properties of slag-CFBC fly ash paste and mortar. *Constr. Build. Mater.* **2014**, *63*, 40–48. [\[CrossRef\]](#)
39. Andersen, M.D.; Jakobsen, H.J.; Skibsted, J. Characterization of white Portland cement hydration and the C-S-H structure in the presence of sodium aluminate by Al and Si MAS NMR spectroscopy. *Cem. Concr. Res.* **2004**, *34*, 857–868. [\[CrossRef\]](#)
40. Rothstein, D.; Thomas, J.J.; Christensen, B.J.; Jennings, H.M. Effect of hydration temperature on the solubility behavior of Ca-, S-, Al-, and Si-bearing solid phases in Portland cement pastes. *Cem. Concr. Res.* **2003**, *33*, 2037–2047.
41. Yang, K.H.; Cho, A.R.; Song, J.K.; Nam, S.H. Hydration products and strength development of calcium hydroxide-based alkali-activated slag mortars. *Constr. Build. Mater.* **2012**, *29*, 410–419. [\[CrossRef\]](#)
42. Guo, X.; Shi, H.; Chen, L.; Dick, W.A. Performance and mechanism of alkali-activated complex binders of high-Ca fly ash and other Ca-bearing materials. In Proceedings of the World of Coal Ash, Lexington, KY, USA, 4–7 May 2009.